42nd AIAA Aerospace Sciences Meeting and Exhibit
5 - 8 January 2004, Reno, Nevada

AIAA 2004-0801

A Sub-grid Mixing Model for Large Eddy Simulation of Supersonic Combustion

V. Sankaran, F. Genin, and S. Menon
School of Aerospace Engineering
Georgia Institute of Technology
Atlanta, Georgia 30332

42nd AIAA/ASME/SAE/ASEE Aerospace Sciences Meeting Jan 5–8, 2004 / Reno, Nevada

A Sub-grid Mixing Model for Large Eddy Simulation of Supersonic Combustion

V. Sankaran*, F. Genin†, and S. Menon‡
School of Aerospace Engineering
Georgia Institute of Technology
Atlanta, Georgia 30332

Abstract

Large eddy simulations of compressible mixing layers have been conducted to investigate scalar mixing at two convective Mach numbers at 0.25 and 0.62. Two sub-grid scalar transport models, one based on a conventional gradient diffusion and the other based on the Linear-Eddy Mixing (LEM) model are used to predict scalar mixing in supersonic flows. It is found that the mixing layer growth is reduced significantly with increase in compressibility, which is consistent with past observations. Numerical predictions obtained using LES-LEM compares very well with the experimental measurements of scalar properties, whereas, the gradient diffusion closure shows significant differences from the measured values. Flow visualizations of density, temperature and mass fraction contours reveal the delay in the formation of the large structures and the growth of the mixing layer as the convective Mach number is increased. Statistics such as mean and the RMS of the velocity and the scalar field exhibit self similarity in the far field. PDF's of the species mass fraction in the supersonic stream become narrow as the compressibility increases, indicating the reduction in mixing.

1 Introduction

As a result of the increasing importance of supersonic combustion, and numerous other technological applications that require mixing in highly compressible flows, there has been a renewed interest in the study of compressible shear layers. Shear layers consist of two parallel streams of same or different species, flowing at same or different speeds on either side of a splitter plate. Fluids from the high and the low speed streams entrain each other, thus stretching the inter-material surface. Formation of fine-scale turbulent structures within the shear layer and especially along the interface further re-distribute the un-mixed fluid and increases the local velocity and scalar gradients. Finally the two streams initially with different momentum, mix at the molecular level by diffusion.

Compressible, single species mixing layers have been experimentally studied extensively in the past.[1–5] These studies have shown that the compressible mixing layers exhibit organized quasi-two dimensional structures similar to their incompressible counter-part, but only when the compressibility effect is low. As the compressibility (or equivalently, the convective Mach Number, M_c) increases, the mixing layer becomes more three-dimensional with drastic reduction in the size and coherence of the quasi-2D organized structures. Past studies have also shown that compressibility increases the stability of the mixing layers and reduces the growth rate, the turbulence intensities and the Reynolds' stresses. Initially, this reduced mixing was attributed to the difference in density between the high and the low speed stream. But later studies[6] showed that even though density has some effect, it is not entirely responsible for the diminished mixing observed in compressible shear layers.

Even though all the experimental data exhibits similar trend regarding the mixing layer growth and the reduction in the turbulence quantities, a considerable scatter exists in the data for a variety of reasons. This includes different experimental facilities and techniques, different definitions of the mixing layer thickness, different initial conditions, differences in the acoustic level in the experimental facilities, etc. This makes it difficult to isolate the effect of compressibility on mixing. In the case of supersonic shear layers, the total pressure has to be manipulated significantly to minimize the formation of waves from the trailing edge of the supersonic section, which is time consuming. In addition, the range of compressibility that can be tested in current experimental facility is limited. This makes it difficult to re-evaluation conclusions from the low M_c regime.

In addition to momentum mixing, scalar mixing is of considerable interest but so far, relatively few scalar measurements have been published for compressible mixing layers. This is because, very good spatial reso-

*Graduate Research Assistant, AIAA Student Member
†Graduate Research Assistant, AIAA Student Member
‡Professor, AIAA Associate Fellow

lution for scalar is very difficult to achieve.[7] Even for moderate Reynolds numbers, achieving adequate resolution to resolve the Batchelor scale is very difficult.[7]

Numerical studies are beginning to complement and further the research on compressible mixing layers. The current work is concerned with the behavior of mixed subsonic-supersonic mixing layers made up of two different species, and the primary objective is to validate a sub-grid model for scalar mixing. The compressible scalar mixing experiments of Clemens et al[5] are simulated and discussed in this paper. Earlier, the velocity measurements in a single specie spatial mixing layer[3] were used to validate momentum mixing using the current LES solver.[8]

The rest of this paper is organized as follows. The governing equations for LES, the sub-grid mixing model and its numerical implementation are explained in the next section. This is followed by the details of the experimental facility and the experimental conditions simulated using the current LES approach. Finally the results obtained from the current study are compared with the experiments, and the advantages and the short-comings of the present sub-grid model are discussed.

2 Governing Equations for LES

The conservation equations of mass momentum, energy and species equations for LES are given by:

$$\begin{array}{ll} \frac{\partial \bar{\rho}}{\partial t} & + \frac{\partial \bar{\rho}\tilde{u}_i}{\partial x_i} = 0 \\ \frac{\partial \bar{\rho}\tilde{u}_i}{\partial t} & + \frac{\partial}{\partial x_j}[\bar{\rho}\tilde{u}_i\tilde{u}_j + \bar{p}\delta_{ij} - \bar{\tau}_{ij} + \tau_{ij}^{sgs}] = 0 \\ \frac{\partial \bar{\rho}\tilde{E}}{\partial t} & + \frac{\partial}{\partial x_i}[(\bar{\rho}\tilde{E} + \bar{p})\tilde{u}_i + \bar{q}_i - \tilde{u}_j\bar{\tau}_{ji} + H_i^{sgs} + \sigma_i^{sgs}] = 0 \\ \frac{\partial \bar{\rho}\tilde{Y}_k}{\partial t} & + \frac{\partial}{\partial x_i}[\bar{\rho}\tilde{Y}_k\tilde{u}_i - \bar{\rho}\tilde{Y}_k\widetilde{V_{i,k}} + Y_{i,k}^{sgs} + \theta_{i,k}^{sgs}] = \bar{\dot{w}}_k \end{array}$$

where $k = 1$ to N_s and N_s is the total number of species present in the system. $\bar{q}_i$ is the heat flux vector given by

$$\bar{q}_i = -\bar{\kappa}\frac{\partial \tilde{T}}{\partial x_i} + \bar{\rho}\sum_{k=1}^{N_s}\tilde{h}_k\tilde{Y}_k\widetilde{V_{i,k}} + \sum_{k=1}^{N_s} q_{i,k}^{sgs} \qquad (1)$$

The diffusion velocities are approximated using Fickian diffusion as $\widetilde{V_{i,k}} = (-\bar{D}_k/\tilde{Y}_k)(\partial\tilde{Y}_k/\partial x_i)$. The sub-grid terms that require closure are:

$$\begin{array}{lcl} \tau_{ij}^{sgs} & = & \bar{\rho}\,(\widetilde{u_iu_j} - \tilde{u}_i\tilde{u}_j) \\ H_i^{sgs} & = & \bar{\rho}\,(\widetilde{Eu_i} - \tilde{E}\tilde{u}_i) + (\overline{pu_i} - \bar{p}\tilde{u}_i) \\ \sigma_i^{sgs} & = & \widetilde{u_j\tau_{ij}} - \tilde{u}_j\bar{\tau}_{ij}. \\ Y_{i,k}^{sgs} & = & \bar{\rho}[\widetilde{u_iY_k} - \tilde{u}_i\tilde{Y}_k] \\ q_{i,k}^{sgs} & = & [\overline{h_kD_k\partial Y_k/\partial x_i} - \tilde{h}_k\tilde{D}_k\partial\tilde{Y}_k/\partial x_i] \\ \theta_{i,k}^{sgs} & = & \bar{\rho}[\widetilde{V_{i,k}Y_k} - \widetilde{V}_{i,k}\tilde{Y}_k] \end{array} \qquad (2)$$

The pressure is determined from the filtered equation of state, $\bar{p} = \bar{\rho}R\tilde{T} + T^{sgs}$. Here, T^{sgs} is the temperature-species correlation term, defined as $[\widetilde{Y_kT} - \tilde{Y}_k\tilde{T}]$. For low heat-release, T^{sgs} can be expected to be negligible[9] but this may not be true for high heat release. However, due to the difficulty in modeling these terms they are generally neglected.[9,10] The filtered total energy per unit volume is given by $\bar{\rho}\tilde{E} = \bar{\rho}\tilde{e} + \frac{1}{2}\bar{\rho}\tilde{u}_i\tilde{u}_i + \bar{\rho}k^{sgs}$ where, the sub-grid kinetic energy (to be discussed later) is defined as, $k^{sgs} = (1/2)[\widetilde{u_ku_k} - \tilde{u}_k\tilde{u}_k]$. The filtered internal energy for calorically perfect gases is given by $\tilde{e} = \sum_{k=1}^{N_s}[c_{v,k}\tilde{Y}_k\tilde{T} + \tilde{Y}_k$ where, $\Delta h_{f,k}^{'} = \Delta h_{f,k}^0 - c_{p,k}T^0$ and $\Delta h_{f,k}^0$ is the standard heat of formation at a reference temperature T^0.

The sub-grid stress tensor τ_{ij}^{sgs} is modeled as follows.

$$\tau_{ij}^{sgs} = -2\rho\nu_t[\tilde{S_{ij}} - \frac{1}{3}\tilde{S_{kk}}\delta_{ij}] + \frac{2}{3}\bar{\rho}k^{sgs}\delta_{ij} \qquad (3)$$

To complete the closure for the sub-grid stresses, the sub-grid eddy viscosity ν_t and the sub-grid kinetic energy, k^{sgs} need to be modeled. A non-equilibrium model[11,12] using a transport equation for the sub-grid kinetic energy, k^{sgs} is used in this study and is given by :

$$\frac{\partial\overline{\rho}k^{sgs}}{\partial t} + \frac{\partial}{\partial x_i}(\overline{\rho}\tilde{u}_ik^{sgs}) = \frac{\partial}{\partial x_i}\left(\overline{\rho}\frac{\nu_t}{Pr_t}\frac{\partial k^{sgs}}{\partial x_i}\right) + P^{sgs} - \epsilon^{sgs} \qquad (4)$$

The terms, P^{sgs} and ϵ^{sgs} in the above equation are respectively, production and dissipation of sub-grid kinetic energy. The sub-grid dissipation, ϵ^{sgs} is obtained by integrating the dissipation spectrum ($D(k) = -2\nu k^2E(k)$) over the unresolved wavenumbers,[13] to get $\epsilon^{sgs} = C_\epsilon\rho(k^{sgs})^{3/2}/\overline{\Delta}$ where, $C_\epsilon = 0.916$. The sub-grid production term is modeled as $P^{sgs} = -\tau_{ij}^{sgs}(\partial\widetilde{u}_i/\partial x_j)$. The coefficient Pr_t is the turbulent Prandtl number and is taken to be 0.9. The sub-grid eddy viscosity is modeled as[13] $\nu_t = C_\nu\sqrt{k^{sgs}}\Delta$, where $C_\nu = 0.067$ nominally. However, both C_ν and C_ϵ can be obtained as a part of the solution by using the dynamical procedure, as shown earlier.[14] In this study, this localized dynamic approach has been used to obtain these coefficients. More information on dynamic modeling can be found elsewhere,[14,15] and therefore, avoided here.

In addition to τ_{ij}^{sgs}, several unclosed terms appear in the LES filtered energy and species equations given in Eqn. (2), such as: H_i^{sgs}: sub-grid enthalpy flux; σ_i^{sgs}: sub-grid viscous work; $Y_{i,k}^{sgs}$: convective species flux; $q_{i,k}^{sgs}$: sub-grid heat flux; $\theta_{i,k}^{sgs}$:sub-grid species diffusive flux;

The sub-grid total enthalpy flux H_i^{sgs} is modeled using the eddy viscosity model as follows: $H_i^{sgs} = (-\overline{\rho}\nu_t/Pr_t)(\partial\tilde{H}_k/\partial x_i)$. Note that, since large-scale motion is resolved in LES, the associated counter-gradient processes in the resolved scales are also re-

solved (even though a gradient closure is employed for H_i^{sgs}).

As noted earlier, a conventional gradient diffusion closure for the scalar equations is employed as a reference sub-grid model to compare with the LEM approach. In this gradient diffusion closure, the sub-grid convective species flux $Y_{i,k}^{sgs}$, given in equation Eqn. [2] is modeled as follows: $Y_{i,k}^{sgs} = (-\overline{\rho}\nu_t/Sc_t)(\partial\tilde{Y}_k/\partial x_i)$ The coefficient Sc_t is the turbulent Schmidt Number, and is taken to be unity.

It should be noted that earlier, theory and experiments[16] have shown that this type of gradient diffusion closure for species transport can lead to significant errors, especially when used in the time-averaged RANS context. Such models are also expected to fail when counter-gradient diffusion occurs. Past studies have shown that counter-gradient diffusion can occur in the present of large-scale coherent structures. As noted above, since the large-scale motion is resolved in a LES, the limitation of a sub-grid eddy diffusivity closure is not that apparent, unless counter-gradient effects occur at the grid scale. Therefore, using this model as a baseline sub-grid closure for LES is acceptable as a first approximation.

The other unclosed terms, σ_i^{sgs}, $q_{i,k}^{sgs}$ and $\theta_{i,k}^{sgs}$, are often neglected in the conventional closure approach, and there exists no model for these terms.[17] These terms are the sub-grid contribution of the molecular diffusive flux and are often neglected assuming that their contributions are small in high Reynolds number flows.[9,10]

It is noted here that most of these assumptions can be relaxed and can be elegantly included in the model for sub-grid scalar transport using the LEM closure described in the next section.

3 Sub-grid Mixing Model

The primary goal of LES is to simulate high Reynolds number flows without resolving the dissipative range of scales. This requires a model for the momentum transport and the scalar transport at the unresolved scales. Models for the sub-grid momentum transport are usually obtained by using the information at the resolved scales, i.e., the unresolved stresses are expressed as a function of resolved field. This works quite successfully for the momentum transport, since the turbulent kinetic energy carried by the dissipative scales are significantly lower than the resolved scales. Unfortunately this is not the case with the sub-grid scalar transport. Molecular diffusion and chemical reaction happens at and below the dissipative range of scales (which are not resolved in LES). Due to the presence of multiple diffusive scalars, and also due to the strong non-linear interaction between the chemical reactions and the turbulence scales, the relation between the sub-grid scalar transport and the resolved-scalar transport is not as straight-forward as the momentum transport. This implies that the sub-grid models developed for the scalar transport must truly represent this multi-scale inter-play of turbulence and combustion to capture the correct physics of combustion.

The issue of simultaneous resolution of the large scale processes (such as large scale convection) and the small scale processes (such as molecular diffusion, turbulent motions near the dissipative scales and chemical reaction) is addressed elegantly using the Linear Eddy Mixing (LEM) model of Kerstein *et al.*[18–21] The basic premise of using LEM in LES (hereafter, referred to as LES-LEM) is that the scalar field evolution can be split into two parts: evolution governed by the large-scale processes and by the small scale processes. Here, the term large and small scales are defined with respect to the filter width defined in the context of LES. As a result, the large-scale processes are defined as those that occur (due to the presence of spatially resolved 3D structures) at and above the filter size and the small-scale processes are the sub-grid turbulent stirring that occur below the LES filter size.

The other physical processes such as the molecular diffusion, the chemical reaction and the volumetric heat release are small-scale processes occurring locally within *each* LES cell. A reduced one-dimensional reaction-diffusion equation is solved inside each LES cell with a resolution fine enough to resolve all turbulent scales from the grid size Δ to the Kolmogorov scale η. The rationale behind this approach and its application in LES has been discussed extensively in the past[13,22,23] and therefore, not repeated here.

It is noted here, however, that since all the physical processes associated with the species field evolution are accounted explicitly in this two-scale (large and small scale) approach, the Eulerian form of the conservation equation of species is not needed. Therefore, in LES-LEM, only mass, momentum and energy equations (in the Eulerian form) are numerically integrated on a three-dimensional grid whereas, the scalar equations are solved using the two-scale approach.

For completeness, some of the salient features of the LEM sub-grid model is described below.

3.1 Sub-grid Reaction-Diffusion

Molecular diffusion and chemical reaction (although not considered here, but included for completeness) evolve on a 1-D line segment known as the "linear-eddy" domain within each LES cell. The following non-conservative form of the reaction-diffusion equations for the species and the temperature are solved on this 1-D line.

$$\rho\frac{\partial Y_k}{\partial t} + F_{k\,stir} + \rho\frac{\partial}{\partial s}(-D_k\frac{\partial Y_k}{\partial s}) = \dot{\omega}_k W_k \qquad (5)$$

$$\rho c_p \frac{\partial T}{\partial t} + F_{T\,stir} - \sum_{k=1}^{N} \rho c_{p,k} D_k (\frac{\partial Y_k}{\partial s})(\frac{\partial T}{\partial s}) - \frac{\partial}{\partial s}(\bar{\kappa}\frac{\partial T}{\partial s}) = -\sum_{k=1}^{N} h_k \dot{\omega}_k W_k \qquad (6)$$

Here, T, $\bar{p}$ and ρ are the sub-grid temperature, resolved pressure, and the sub-grid mass density, respectively. Y_k, W_k, $c_{p,k}$ and R_u, are the mass fraction, molecular weight, specific heat at constant pressure, and universal gas constant respectively. Density in the sub-grid field is computed using the equation of state for the scalar mixture $\bar{p} = \rho T \sum_{k=1}^{N} Y_k R_u / W_k$ and the caloric relation is given by $h_k = \Delta h^o_{f,k} + \int_{T^o}^{T} c_{p,k}(T')dT'$. Also, $\dot{\omega}_k$, h_k, V_k and $\Delta h^o_{f,k}$ are respectively the mass reaction rate, enthalpy, diffusion velocity and standard heat of formation (at standard temperature, T^o) of the k-th species. $\bar{c}_p$, $\bar{\kappa}$ and D_k are the mixture averaged specific heat at constant pressure and thermal conductivity and mixture averaged diffusivity of the k-th species respectively.

In Eqns. [5] and [6], s denotes the co-ordinate direction on the 1-D domain. The orientation of the 1-D domain is usually aligned in the direction of the maximum scalar gradient.[19] The length of the 1-D domain is taken to be equal to that of the local LES filter width, Δ. Turbulent convection at the sub-grid scales of the form $u\partial Y_k/\partial s$ and $u\partial T/\partial s$ are symbolically represented as $F_{k\,stir}$ and $F_{T\,stir}$, respectively in Eqns. [5] and [6] and these are implemented explicitly, as discussed in the next section.

The following assumptions have been made in arriving at the above formulation: (1) sub-grid pressure (inside the 1-D LEM domain) is assumed to be uniform and same as the resolved grid pressure. This assumption can be questionable in the presence of high compressibility, and its accuracy remains to be evaluated, (2) the contribution from the sub-grid viscous work is neglected, (3) calorically perfect gas model is currently assumed, but it is straight-forward to extend LEM for thermally perfect gas, and (4) radiation effects are neglected in this study but can be easily included, as shown elsewhere.[24]

3.2 Sub-grid turbulent convection

The effects of the sub-grid velocity field on the sub-grid scalar fields are modeled (numerically) using stochastic re-arrangement events called *triplet maps*.[19] Each triplet map represents an instantaneous action of an isotropic turbulent eddy on the sub-grid scalar field. The scalar field produced is continuous and measure preserving (Note: scalar gradient field is not continuous). In essence, triplet map increases the sub-grid scalar gradient by a mechanism similar to the compressive strain rate in turbulent flow, consistent with the DNS notions of Ashurst.[25]

The three important parameters of the sub-grid turbulent stirring are the eddy size l, the eddy location (within the sub-grid 1-D domain) and the stirring frequency (mean event rate per unit length of the mapping domain) λ. These parameters are suitably constrained, so as to obey the turbulent-transport-scaling governed by the Kolmogorov cascade picture in a statistical sense. The eddy size in the range Δ to η (Kolmogorov scale) is determined from an eddy size distribution $f(l)$, obtained using inertial range scaling in three-dimensional turbulence:[19]

$$f(l) = \frac{5}{3}\frac{l^{-8/3}}{(\eta^{-5/3} - \Delta^{-5/3})} \qquad (7)$$

Here, η is determined from inertial range scaling law

$$\eta = N_\eta \frac{\Delta}{Re_\Delta^{3/4}} \qquad (8)$$

where N_η is an empirical constant and Re_Δ is the sub-grid Reynolds' number based on the sub-grid turbulence intensity, kinematic viscosity and the local LES filter width, Δ. The constant N_η reduces the effective range of scales between Δ and η but does not change the turbulent diffusivity, as described in an earlier study.[26] The two constants: C_λ and N_η, arising from the use of scaling laws can be determined dynamically. However, the present study, uses a constant value reported in the earlier studies.[26,27]

The event location is randomly chosen from a uniform distribution and the event (mapping) rate (mean frequency per unit length) is[19]

$$\lambda = \frac{54}{5}\frac{\nu Re_\Delta}{C_\lambda \Delta^3}\frac{[(\Delta/\eta)^{5/3} - 1]}{[1 - (\eta/\Delta)^{4/3}]} \qquad (9)$$

The time interval between events is then given as $\Delta t_{stir} = 1/\lambda\Delta$ where Δ is the length of the 1-D domain, which is also same as the local LES filter width. These mappings are implemented as a Poisson process in time. Note, that λ is not a function of length scale, l (of stirring) which implies that the interval between the stirring events are the same for all the length scales. Strictly speaking this is not true, but the following considerations justify the proposition.
(1) Assumption of the local isotropy in the sub-grid, implies that the range of the stirring length scales are closely spaced in the wave-number space. This implies that their time-scale (or the turn-over time) is nearly same.
(2) The sub-grid Re_Δ and the filter width, Δ are varying spatially over the LES (resolved) grid. This implies that the the range of the stirring length scales and hence, the frequency of the stirring events also vary spatially over the LES (resolved) grid, even though it is same within the sub-grid.

Since, the inertial range properties are built into the equations for the eddy-size PDF and the eddy-frequency parameter, λ, Kerstein[20] showed that LEM

is able to capture the correct exponential increase of an iso-scalar (level-sets) lines in accordance with the Batchelor's theory.

3.3 Volumetric Expansion

The final sub-grid process in the LEM, which needs to be described is the volumetric expansion due to density change. This change can occur due to heat release or due to sub-grid compressibility. In the present study, since there is no chemical reaction and heat release, and therefore, this effect does not have to be included. An assumption in the current study is that the sub-grid pressure is constant. This assumption may not be strictly true in highly compressible flow where sub-grid compressibility can vary from LES cell to cell. For example, presence of a shock wave can result in this effect. At present, this issue has not yet been addressed and is not needed for the current study since the experimental setup employed pressure matched streams to ensure no shocks.

3.4 Numerical Implementation

An operator splitting method[26,28] is used to integrate the stiff reaction-diffusion equations (Eqns. [5] and [6]). This splitting combines an explicit treatment of the LES resolved mass and momentum equations at the global time step with several explicit fractional steps for diffusion, reaction and turbulent stirring at the sub-grid scales. Thus, the idea behind operator-splitting technique is the sequential application of individual operators at the respective time-scale of the operator in such a way as to ensure accuracy and numerical stability of the computation.

In LES-LEM, each of these operators, namely molecular diffusion, chemical reaction, thermal expansion and turbulent convection are implemented numerically as discrete events in time. The epoch or the instant at which each of these processes need to be implemented depends on the respective time-scale of each of these processes. These time-scales are identified below.

Diffusion time scale - Δt_{diff}: Time scale associated with the transport of species and temperature from a region of higher concentration to a lower concentration due to random motion of the molecules. This is the slowest physical process among the other sub-grid processes and is computed as $\Delta t_{diff} = \kappa \Delta s^2 / max[D_k]$ where, Δs is the LEM grid size and D_k is the mass diffusivity of the species "k". κ is set to 0.25 for numerical stability.

Stirring time scale - Δt_{stir}: Time scale associated with the sub-grid turbulent convection, is estimated as $\Delta t_{stir} = 1/\lambda\Delta$. This is the time-scale at which the triplet maps are implemented. It is a strong function of sub-grid Reynolds number Re_Δ, i.e., higher Re_Δ implies a smaller stirring time scale.

To solve the Eqns. [5] and [6] numerically, all spatial derivatives are discretized using a second-order accurate central difference schemes, and a zero-gradient boundary conditions are imposed for the species and the temperature equations at sub-grid domain boundaries.

LEM-domain (1-D line segment) is initialized in every LES cell with a fixed number of cells. The number of one-dimensional cells is estimated as follows. To represent an eddy using a triplet map, a minimum of 6 points are needed.[29] If the sub-grid Re_Δ is known, then using the expression $\eta = N_\eta \Delta Re_\Delta^{-3/4}$, an estimate of the smallest length scale can be obtained. Then the maximum number of LEM cells needed to completely resolve all the sub-grid scales can be computed using the expression, $N_{max} = \min(\Delta_{ijk}/\eta_{ijk})$ where Δ_{ijk} and η_{ijk} are the local LES filter width and the Kolmogorov scale at the cell "ijk". The length of the linear eddy domain is set equal to the LES filter width Δ.

3.5 Large-Scale Convection: Splicing

The large-scale convection process is implemented using a Lagrangian approach called **splicing**. After completing the sub-grid LEM simulations in each LES cell, the sub-grid scalar fields are convected by the LES-resolved velocity field, in a Lagrangian sense. This method involves the transfer of LEM cells between the LES control volumes to account for the mass flux across the LES cell faces. Three quantities are needed for this procedure: (1) magnitude or the amount of mass that has to be transported across each of the LES cell faces, (2) direction of the mass flux (influx or outflux) on each cell face, (3) ordering/priority of the convection operation for the 3-co-ordinate directions

In a finite-volume scheme, mass flux is known on each of the LES cell faces. In addition, the direction of the velocity field defines the direction of the mass flux on the cell-faces. Hence, the first two of the above mentioned three quantities are taken care of by the resolved grid continuity equation and the momentum equations. The third issue is resolved using the following approach.

In the numerical implementation of the scalar convection, the three dimensional convection operator is approximated by a sequence of three, one-dimensional convection operators. On a general three-dimensional grid the mass transfer from any control volume to any neighboring control volume is also predominantly three-dimensional. As a result, different number of one-dimensional cells are transported in different spatial directions. So the order in which these operators act on the scalar field can have a significant effect on the scalar field evolution. Here, the cells going out in the direction of largest outflux are fluxed out first from the right end of the sub-grid domain. Similarly the largest influx is added first to the left end of one-dimensional domain.

Next step in the large-scale convection process is the identification and actual transport of the linear-eddy cells. This is implemented as follows. Since the mass flux on each of the six control surfaces of a LES cell is known, it can be sorted in an ascending order. Note that, before sorting the following sign-convention is imposed for the face mass-fluxes. Influx is given a positive sign and the outflux is given a negative sign along each co-ordinate directions. Thus, upon sorting, the mass fluxes would be arranged, from the maximum outflux (least negative number) to maximum influx (highest positive number). Now, for each outflux, every LES cell computes the number of one-dimensional cells that contains the mass. Since the density and the volume is known for each one-dimensional cell, the cell mass is computed simply as the product of the cell density times the cell volume. It should be noted that, the amount of mass to be transported across a LES cell surface can be a fraction of the linear eddy cell mass. To transport mass smaller than the cell mass, the following algorithm is used.

- Let the temperature and mass fraction of the linear-eddy cell D be T_D and Y_{k_D}
- Let the density, volume and the mass of the cell D be ρ_D, V_D and Δm_D
- Let the amount of mass to be transported across an LES cell surface be δm
- If $\delta m < \Delta m_D$, then split D into two cells, D_L and D_R such that,
  $\rho_{D_L} = \rho_{D_R} = \rho_D$
  $\Delta m_{D_R} = \delta m$
  $\Delta m_{D_L} = \Delta m_D - \delta m$
  $V_{D_R} = \delta m / \rho_D$
  $V_{D_L} = V_D - V_{D_R}$
  $T_{D_L} = T_{D_R} = T_D$
  $Y_{k_{D_L}} = Y_{k_{D_R}} = Y_{k_D}$

3.6 Large-Scale and Small-Scale Coupling

To complete the LES-LEM formulation, the simulated sub-grid field must be coupled to the LES-resolved variables. The resolved field provides the pressure and the sub-grid kinetic energy to the sub-grid LEM simulation. After the sub-grid simulation, the sub-grid LEM field provides the filtered species, temperature and the specific heats to the resolved field.

Filtered quantities from the sub-grid simulation are computed as follows.

- Let Y_{k_i} be the sub-grid species mass fraction for species 'k' in a cell 'i'
- Let T_i and ρ_i be the sub-grid temperature and density in a cell 'i'
- Sub-grid averaged (filtered)species mass fraction is computed as
  $\widetilde{Y_{k_i}} = \sum_{i=1}^{N_{LEM}} \rho_i Y_{k_i} \; / \; \sum_{i=1}^{N_{LEM}} \rho_i$
- Sub-grid averaged (filtered) temperature is computed as
  $\widetilde{T_i} = \sum_{i=1}^{N_{LEM}} \rho_i T_i \; / \; \sum_{i=1}^{N_{LEM}} \rho_i$

This sub-grid averaged (filtered) temperature is redundant, since the solution of the LES-resolved energy equation along with the filtered species (from LEM) gives the actual temperature. The LES-resolved temperature actually includes the effect of resolved viscous work (this part is missing in the sub-grid LEM). In the actual simulation, both temperatures are computed and compared. In general, the comparison show that both these temperatures are in very good agreement with each other, suggesting that at least for the problem studied here viscous work effect is relatively small.

Table 1 Test Cases simulated here[5]

Parameter	$M_c = 0.28$	$M_c = 0.62$	$M_c = 0.79$
M_1	1.64	2.0	2.2
M_2	0.91	0.4	0.39
$U_1(m/s)$	430	480	508
$U_2(m/s)$	275	130	110
$T_1(K)$	172	150	140
$T_2(K)$	223	252	253
$P_{O_1}(Kpa)$	302	495	600
$P_{O_2}(Kpa)$	115	75	67
ρ_2/ρ_1	0.77	0.59	0.77
U_2/U_1	0.63	0.27	0.22
λ_B μm	1.7	0.8	0.7
Resolution	$2-7\ \lambda_B$	$5-14\ \lambda_B$	$5-16\lambda_B$

4 Experimental Conditions

The experimental facility consisted of a wind tunnel with a plenum section, nozzle, a test section and a diffuser. The rectangular test section where the measurements were taken, is 10 cm wide, 8 cm high and 48 cm long. The high (supersonic) and the low (subsonic) speed streams separated by the splitter plate flows into the constant area test section from the top and the bottom sides of the splitter plate respectively. Upstream of the test section, a nozzle housing a centerbody with supersonic and subsonic contours were used to provide nearly uniform exit conditions.

The principal diagnostics used in the experimental study were Pitot pressure, static pressure, Schlieren, Planar Mie scattering for flow visualization, Planar Laser Induced Florescence (PLIF) for scalar measurements and Laser Doppler Velocimetry (LDV) for velocity measurements. The simulation parameters are listed in Table 1

Based on the high speed nozzle exit momentum Reynolds number, Re_{θ_1} (> 7200), the boundary layer at the tip of the splitter plate is expected to be turbulent.[5] The convective Mach number, M_c is the

measure of the compressibility of the mixing layer[30] and is defined as the Mach number with respect to a frame of reference traveling with the average large scale structures in the flow. Three cases are simulated in the current study, ranging from low to high compressibility.

5 Grid & Boundary Conditions

The numerical simulation reported here uses a 181 $\times$ 150 $\times$ 5 grid in the stream wise, transverse and span wise directions. The computational domain is 50 cm long and 8 cm high. The grid points were clustered near the splitter plate in the stream wise and transverse direction. Based on the incoming boundary layer profiles, this provided a resolution of $y^+ = 15$ on either side of the splitter plate. The bottom and top walls of the test section was resolved using a $y^+ = 45$. The thickness of the splitter plate trailing edge (0.8 mm) is resolved using 7 equally spaced grid points. Grid spacing in the span wise direction is uniform and set equal to the axial spacing at the splitter plate edge. Since only a few grid points are used in the span wise direction, the current simulations are unable to resolve any long wavelength disturbance in the spanwise direction. The current simulations also preclude inclusion of any highly oblique waves in the shear layer. Future studies will address the issue of span wise waves in more details.

All boundary conditions are specified to closely match the experiments.[5] For the supersonic stream, all conditions are specified and for the subsonic stream, characteristic inflow conditions[31] are specified. An inflow turbulence intensity of 2 % is used for the both the streams. At the outflow plane, because of the presence of a mixed supersonic-subsonic flow, a mixed boundary condition is applied. Based on the local Mach number at the outflow, an extrapolation (where the flow is supersonic) or a Poinsot-Lele[31] (where the flow is subsonic) boundary condition was applied. No-slip, adiabatic conditions is applied at the top and the bottom walls and slip boundary condition is applied in the span wise direction to allow for the three dimensionality of the flow in that direction.

The number of LEM cells needed for the simulation is governed by the scalar field resolution. A measure of the scalar resolution is given by the Batchelor scale (a characteristic size of the smallest scalar fluctuation),[5,32] defined as $\lambda_B \approx 25\delta_w Re_w^{-3/4} Sc^{-1/2}$. Here, δ_w is the vorticity thickness, Re_w is the Reynolds' number based on the vorticity thickness, and Sc is the Schmidt number. The LEM resolution ($\Delta_{LEM} = \Delta_{LES}/12$) used here provides a grid spacing of $\Delta_{LEM_1} = 3.7\mu m$ in the supersonic stream and $\Delta_{LEM_2} = 11.5\mu m$ in the subsonic stream.

Table 1 shows the average Bachelor scale, λ_B for the three convective Mach number simulated as reported by Island.[7] In comparison, the LEM grid spacing employed in the present study resolves $2 - 5\lambda_B$ on the supersonic side and $7 - 16\lambda_B$ on the subsonic side, which is considered reasonable.

The current simulations are carried out on a distributed memory parallel processing computer (Intel Xeon, 2.6 GHz) using the Message Passing Interface (MPI). Typically, 24 processors are employed and the memory requirement is 2.4 Gigabytes. For the present simulations, using 135750 LES grid points and 12 LEM cells per LES cell, 96 single processor hours are required per flow through time.

6 Results and Discussion

In the following discussion, LES-GRAD-DIFF is used to denote the gradient diffusion sub-grid closure and LES-LEM is used to denote the subgrid LEM closure.

6.1 Velocity Profiles

The experiments on scalar mixing[5] report only the scalar measurements. Therefore, to compare the velocity field, data from an earlier experimental study from the same group[33] have been used here. The experimental facility and most of the conditions[33] are very similar to the scalar studies[5] experiments. Planar velocity measurements at $M_c = 0.25$ and 0.63 were reported in the earlier experiments,[33] and their results compared directly with the current LES at $M_c = 0.28$ and 0.62 (for which scalar measurements have been reported).

As noted earlier, the mixing layer growth rate is significantly affected by compressibility effect. Figure 1 shows the axial variation of the mixing layer thickness for the three cases simulated. It should be noted that to compute the growth rate, mixing layer thickness data are obtained only from the regions where the mean axial velocity has attained self-similarity. Elliot *et al*[3] suggested that self-similarity is achieved anywhere from 350 to 1000 momentum thicknesses from the trailing edge of the splitter plate. Following this definition and based on the inlet momentum thickness of $\theta = 0.14mm$[5] the slope of the mixing layer thickness between x = 350 $\theta = 0.05m$ and x = 1000 $\theta = 0.14m$ is computed to be $d\delta/dx = 0.043$ for $M_c = 0.28$ and 0.051 for $M_c = 0.62$. These are in reasonable agreement with the experimental prediction of the growth rate of 0.036 and 0.061.[5] The compressible growth rate normalized by the incompressible growth rate seems to decrease with increasing convective Mach number consistent with the past observation. For example, for a given velocity ratio ($r = U_2/U_1$) and density ratio ($s = \rho_2/\rho_1$), the growth rate for the incompressible mixing layer is given by,[1] $d\delta/dx = C_\delta(1-r)(1+\sqrt{s})/(1+r\sqrt{s})$, where C_δ is a constant equal to 0.14.[5] Based on this estimate, the growth rate of the incompressible mixing layer for the same velocity and density ratio as the compressible mixing layers simulated here, are

$d\delta/dx = 0.062$ and 0.14878 for $M_c = 0.28$ and 0.62, respectively. Therefore the ratio of compressible to incompressible growth rate for the two M_C's are 0.6935 and 0.3427, which is in good agreement with the past studies as shown in fig. 2.

Figures 3(a) and (b) show respectively, the normalized axial mean velocity profiles as a function of the similarity co-ordinate $\eta = (y - Y_c)/\delta$ for $M_c = 0.25$ and $M_c = 0.62$, respectively. Axial velocity is normalized as $u - U_2/(U_1 - U_2)$, where U_1 and U_2 are the velocity of the supersonic and subsonic streams, respectively. Also, Y_c is the transverse location where $u - U_2/(U_1 - U_2)$ is 0.5 and δ is the thickness of the mixing layer defined as the distance between the transverse locations where $u - U_2/(U_1 - U_2)$ is 0.95 and 0.05. With this normalization the axial velocity profiles at various downstream locations collapse together, thereby exhibiting self-similarity. It can also be observed in Fig. 3 that the numerical prediction by both LES-LEM and LES-GRAD-DIFF compares very well with the experiments.

Figures 4(a) and (b) show respectively, the corresponding axial root-mean-square (RMS) velocity profiles. Experimental data shows that the peak axial RMS velocity decreases with increasing M_c. The lower M_c case under predicts the peak by about 25 %. At present, this is reason behind this discrepancy is unresolved and may be related to the differences in M_c (0.28 v.s 0.25) or the grid resolution. There is substantial deviation from the measurements at the outer edges of the mixing layer for all the current results. This may be an indication that that the intermittency at the shear layer edge is not properly resolved in the current simulations.

Finally, Figs. 5(a) and (b) show respectively, the corresponding normalized Reynolds stresses for the two cases. The current LES results are in reasonable agreement with the experiments. The predicted peak Reynolds stress decreases with increase in M_c, a trend consistent with experiments.[3,4,33] However, the peak is under-predicted at the high M_c by both the LES closures.

In general, the predicted velocity field is in reasonable agreement with data for both the sub-grid closures (LES-GRAD-DIFF and LES-LEM) studied here. This suggests that, at least for these test cases, LES with gradient diffusion is reasonably accurate for predicting the variation of the momentum mixing layer. This may be a result of the fact that in LES, all the scales of motion (even counter-gradient ones) are resolved on the LES grid. These results also suggest that the scalar closure for the current conditions has very little effect on the momentum transport and mixing. Note that the momentum closure is the same for both the test cases.

6.2 Scalar Profiles

The scalar mixing analysis suggests a more fundamental test of the two closures test here since they are substantially different in approach and implementation. The LES-GRAD-DIFF closure is imposed on a scalar field that is resolved only at the LES grid level whereas, the LES-LEM model simulated both the sub-grid (i.e., below the LES grid level) and the LES-resolved processes. As a results, subtle features resulting from sub-grid processes (if relevant) should show up in the latter approach.

Figures 6 (a) and (b) show respectively, the profiles of mean and the RMS fluctuations of the species mass fraction in the supersonic stream for the two M_c cases. In the experiments,[5] mean and the RMS of the mixture fraction were calculated from the probability density functions (PDF) of the mixture fraction. In the current study, instantaneous data collected over a long period is ensemble-averaged to obtain the mean and the RMS mass fractions. As shown, LES-LEM prediction is in excellent agreement with the experiments for cases where data is available ($M_c = 0.25$, 0.62). On the other hand, the gradient diffusion model (LES-GRAD-DIFF) prediction deviates substantially from the measured data, especially in the high speed upper stream for the mean mixture fraction and the peak rms fluctuation is also over predicted.

Finally, Figs. 7 (a) and (b) show respectively, the PDF of the species mass fraction in the supersonic stream at the transverse location corresponding to the similarity coordinate $\eta = 0$. The overall agreement of the LES-LEM with the experimental data is again encouraging. Accurate prediction of the PDF of the mixture fraction implies that all the higher moments (e.g., mean and the RMS) can now be computed accurately. In contrast, LES with gradient diffusion closure predicts a much broader PDF with a lower peak indicating a diffusive nature of the solution.

7 Conclusion

LES of mixed supersonic-subsonic compressible mixing layers have been carried out using a conventional sub-grid eddy diffusion closure and a sub-grid simulation model based on LEM. Results for two convective Mach numbers are compared to available data in terms of both velocity and scalar profiles. It is shown that, at least for the cases simulated here, both scalar closures predict similar momentum mixing profiles, thus suggesting that even simple eddy diffusion closures can provide reasonable results for the velocity field. Analysis of the scalar mixture fraction mean and rms profiles, however, shows that the LES-LEM closure is able to better predict the scalar profiles, thereby suggesting that scalar processes at the sub-grid level play an important role in the overall evolution of the mixing layer.

Additional studies are still warranted to address

some of the unresolved issues. Effect of heat release is ignored in this study but the LES-LEM has shown promise in reacting flows in earlier studies in subsonic flows[13,23] and its ability in supersonic combustion was recently investigated[34] but still needs to be fully investigated. Nevertheless, the current study along with the earlier studies using LES-LEM suggest that this closure has some unique features that are not constrained by flow or geometrical conditions. As a result, it has the potential for wide applications in both subsonic and supersonic mixing and combustion.

Acknowledgments

This work was supported in part by the NASA Glenn Research Center NRA and by NASA URETI Institute for Future Space Transport.

References

[1] Papamoschou, D. and Roshko, A., "The compressible turbulent shear layer:an experimental study," *Journal of Fluid Mechanics*, Vol. 197, 1998, pp. 453–477.

[2] Dimotakis, P. E., "On the convective velocity of turbulent structures in supersonic sher layers," *AIAA-91-1724, 29th Aerospace Sciences Meeting, Reno, NV.*, 1991.

[3] Elliott, G. S. and Samimy, M., "Compressibility effects in free shear layers," *Physics of Fluids*, Vol. 2, 1990, pp. 1231–1240.

[4] Goebel, S. G. and Dutton, J. C., "Experimental study of compressible turbulent mixing layers," *AIAA Journal*, Vol. 29, 1991, pp. 538–546.

[5] Clemens, N. T. and Mungal, M. G., "Large-scale-structure and entrainment in the supersonic mixing layer," *Journal of Fluid Mechanics*, Vol. 284, 1995, pp. 171–216.

[6] Brown, G. L. and Roshko, A., "On Density effects and Large Structures in Turbulent Mixing Layers," *Journal of Fluid Mechanics*, Vol. 84, 1974, pp. 775–816.

[7] Island, T. C., *Quantitative scalar measurements and mixing enhancement in compressible shear layers*, Ph.D. thesis, Stanford University, Mechanical Engineering Department, CA, April 1997.

[8] Nelson, C. C., *Simulations of spatially evolving compressible turbulence using a local dynamic subgrid model*, Ph.D. thesis, Georgia Institute of Technology, Atlanta, GA, December 1997.

[9] Fureby, C., *On Modelling of Unsteady Combustion utilizing Continuum Mechanical mixture Theories and Large Eddy Simulations*, Ph.D. thesis, Lund Institute of Technology, Sweden, 1995.

[10] Veynante, D. and Poinsot, T., "Reynolds Averaged and Large Eddy Simulation Modelling for Turbulent Combustion," *New Tools in Turbulence ModeLling*, edited by O. Metais and J. Ferziger, Springer-Les Editions De Physique, 1996.

[11] Schumann, U., "Subgrid Scale Model for Finite Difference Simulations of turbulent Flows in Plane Channels and Annuli," *Journal of Computational Physics*, Vol. 18, 1975, pp. 376–404.

[12] Menon, S., Yeung, P.-K., and Kim, W.-W., "Effect of Subgrid Models on the Computed Interscale Energy Transfer in Isotropic Turbulence," *Computers and Fluids*, Vol. 25, No. 2, 1996, pp. 165–180.

[13] Chakravarthy, V. and Menon, S., "Subgrid Modeling of Premixed Flames in the Flamelet Regime," *Flow, Turbulence and Combustion*, Vol. 65, 2000, pp. 133–161.

[14] Kim, W.-W., Menon, S., and Mongia, H. C., "Large Eddy Simulations of a Gas Turbine Combustor Flow," *Combustion Science and Technology*, Vol. 143, 1999, pp. 25–62.

[15] Kim, W.-W. and Menon, S., "A New Incompressible Solver for Large-Eddy Simulations," *International Journal of Numerical Fluid Mechanics*, Vol. 31, 1999, pp. 983–1017.

[16] Dimotakis, P. E., "Turbulent Free shear layer Mixing," *AIAA-89-0262*, 1989.

[17] Poinsot, T. and Veynante, D., *Theoretical and Numerical Combustion*, Edwards, Inc., 2001.

[18] Kerstein, A. R., "Linear-Eddy Model of Turbulent Scalar Transport and Mixing," *Combustion Science and Technology*, Vol. 60, 1988, pp. 391–421.

[19] Kerstein, A. R., "Linear-Eddy Model of Turbulent Transport II," *Combustion and Flame*, Vol. 75, 1989, pp. 397–413.

[20] Kerstein, A. R., "Linear-Eddy Modeling of Turbulent Transport. Part 6. Microstructure of Diffusive Scalar Mixing Fields," *Journal of Fluid Mechanics*, Vol. 231, 1991, pp. 361–394.

[21] Kerstein, A. R., "Linear-Eddy Modeling of Turbulent Transport. Part V: Geometry of Scalar Interfaces," *Physics of Fluids A*, Vol. 3, No. 5, 1991, pp. 1110–1114.

[22] Chakravarthy, V. and Menon, S., "Large-Eddy Simulations of Turbulent Premixed Flames in the Flamelet Regime," *Combustion Science and Technology*, Vol. 162, 2001, pp. 175–222.

[23] Sankaran, V. and Menon, S., "Vorticity-scalar alignments and small-scale structures in swirling spray combustion," *Proceedings of the Combustion Institute*, Vol. 29, 2003, pp. 577–584.

[24] Zimberg, M. H., Frankel, S. H., Gore, J. P., and Sivathanu, Y. R., "A Study of Coupled Turbulent Mixing, Soot Chemistry and Radiation Effects Using the Linear Eddy Model," *Combustion and Flame*, Vol. 113, 1998, pp. 454–469.

[25] Ashurst, W. T., Kerstein, A. R. Kerr, R. M., and Gibson, "Alignment of Vorticity and Scalar gradient with strain rate in simulated Navier Stokes turbulence," *Physics of Fluids*, Vol. 30, 1987, pp. 2343–2353.

[26] Smith, T. and Menon, S., "One-Dimensional Simulations of Freely Propagating Turbulent Premixed Flames," *Combustion Science and Technology*, Vol. 128, 1996, pp. 99–130.

[27] Smith, T. M. and Menon, S., "Model Simulations of Freely Propagating Turbulent Premixed Flames," *Proceedings of the Combustion Institute*, Vol. 26, 1996, pp. 299–306.

[28] Calhoon, W. H., Menon, S., and Goldin, G., "Comparison of Reduced and Full Chemical Mechanisms for Nonpremixed Turbulent H2-Air Jet Flames," *Combustion Science and Technology*, Vol. 104, 1995, pp. 115–141.

[29] Menon, S. and Calhoon, W., "Subgrid Mixing and Molecular Transport Modeling for Large-Eddy Simulations of Turbulent Reacting Flows," *Proceedings of the Combustion Institute*, Vol. 26, 1996, pp. 59–66.

[30] Bogdanoff, D. W., "Compressibility effects in turbulent shear layers," *AIAA Journal*, Vol. 321, No. 6, 1983, pp. 926–927.

[31] Poinsot, T. and Lele, S., "Boundary Conditions for Direct Simulations of Compressible Viscous Flow," *Journal of Computational Physics*, Vol. 101, 1992, pp. 104–129.

[32] Koochesfahani, M. M. and Dimotakis, P. E., "Mixing and Chemical reactions in a turbulent liquid mixing layer," *Journal of Fluid Mechanics*, Vol. 170, 1986, pp. 83–112.

[33] Urban, W. D., *Planar Velocity Measurements in compressible mixing layers*, Ph.D. thesis, Stanford University, March 1999.

[34] Genin, F., Chernyavsky, B., and Menon, S., "Large eddy simulation of scramjet combustion using a subgrid mixing/combustion model," *AIAA-2003-7035*, 2003.

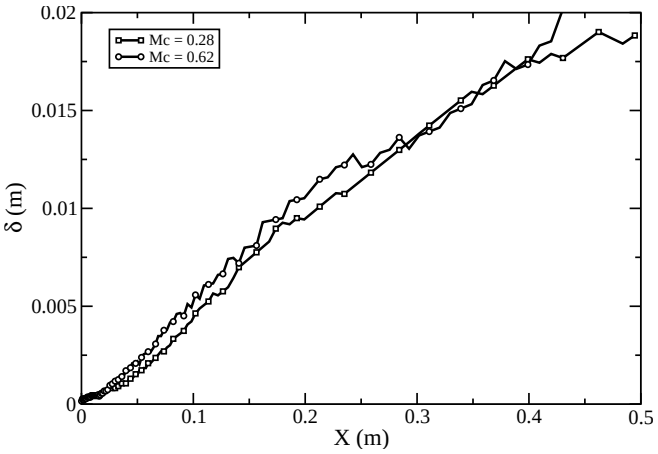

Figure 1 Axial variation of the mixing layer thickness for various M_C.

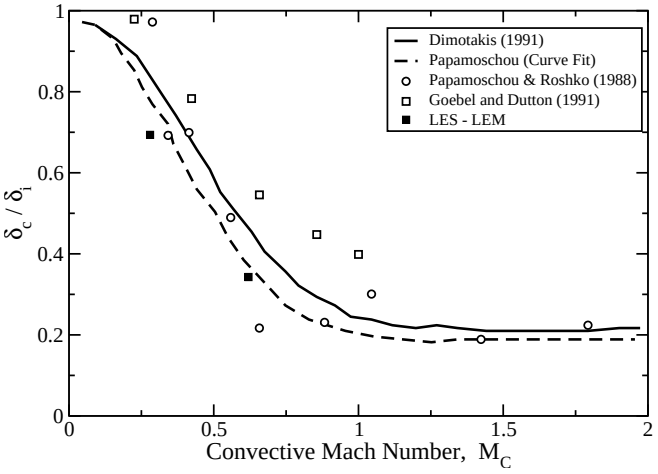

Figure 2 Normalized Growth rate as a function of convective Mach number. Here, δ_c is the compressible mixing layer thickness and δ_i is the incompressible mixing layer thickness.

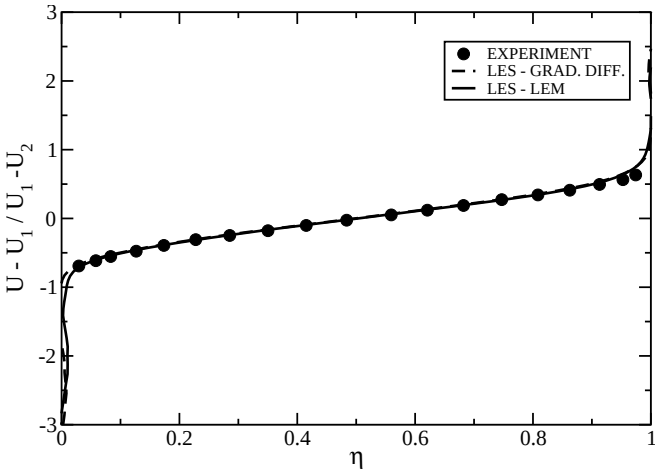

a) $M_c = 0.25$

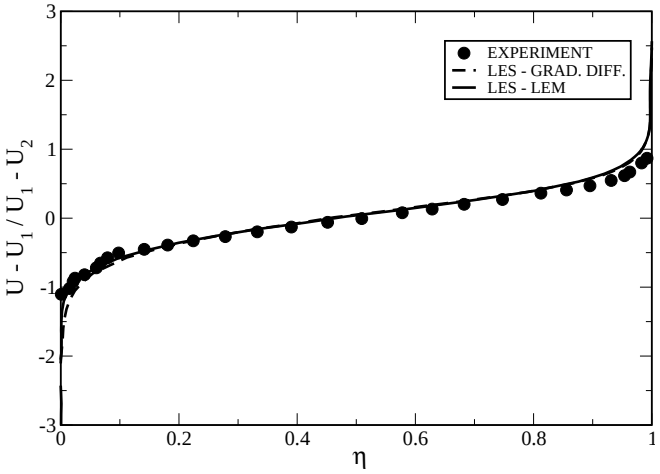

b) $M_c = 0.62$

Figure 3 Transverse profiles of mean axial velocity.

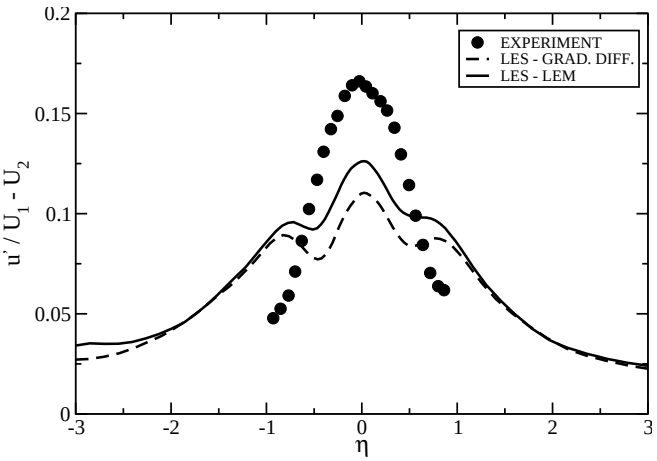

a) $M_c = 0.25$

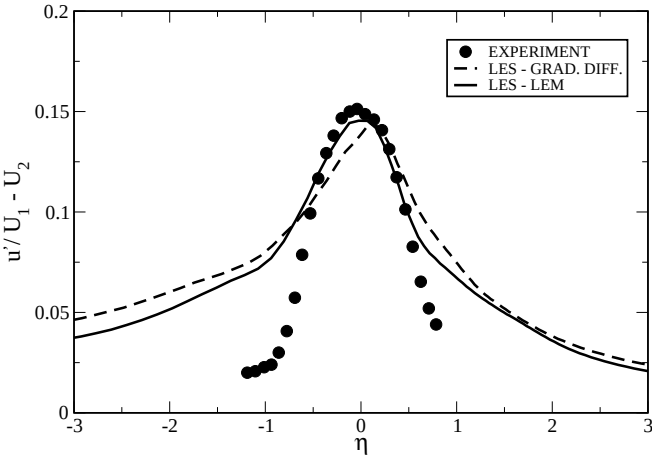

b) $M_c = 0.62$

Figure 4 Transverse profiles of rms axial velocity.

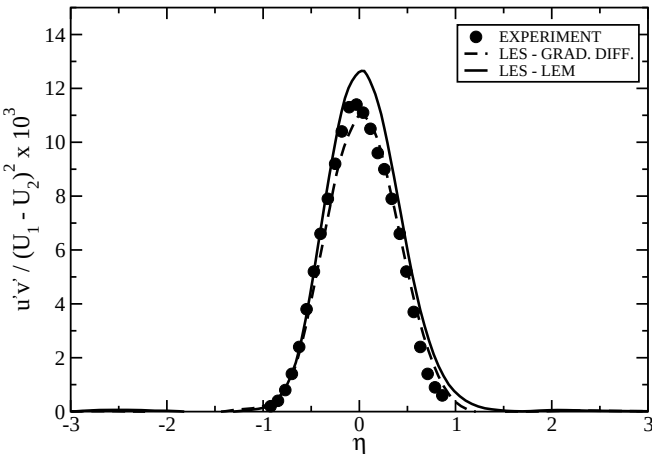

a) $M_c = 0.25$

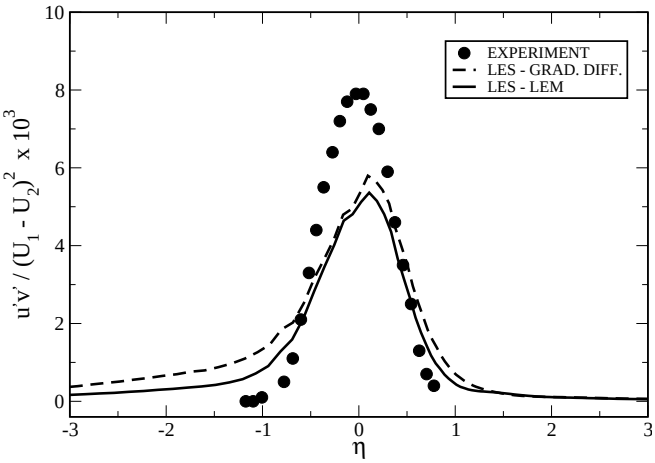

b) $M_c = 0.62$

Figure 5 Transverse profiles of Reynolds' stress.

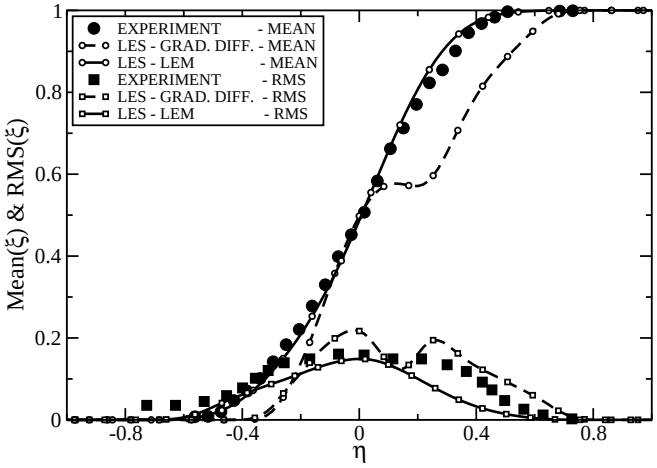

a) $M_c = 0.25$

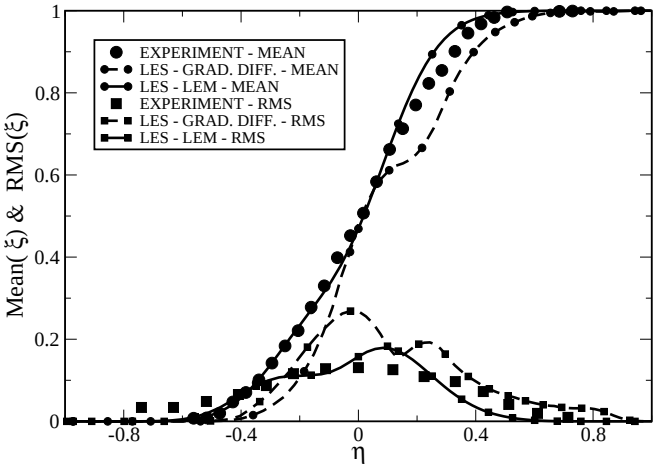

b) $M_c = 0.62$

Figure 6 Transverse profiles of mean and rms mixture fraction.

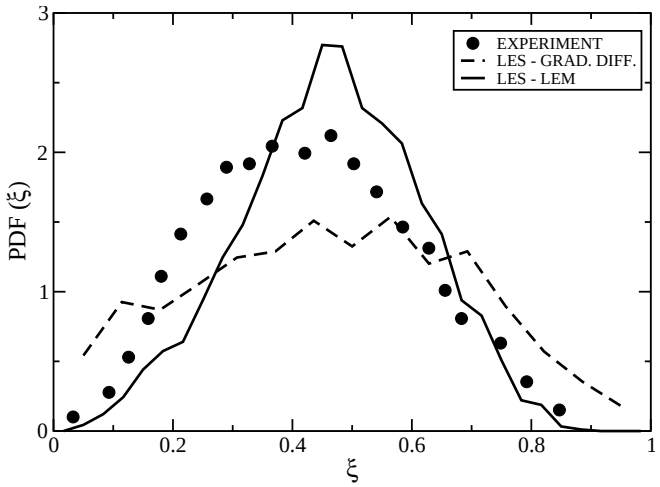

a) $M_C = 0.25$

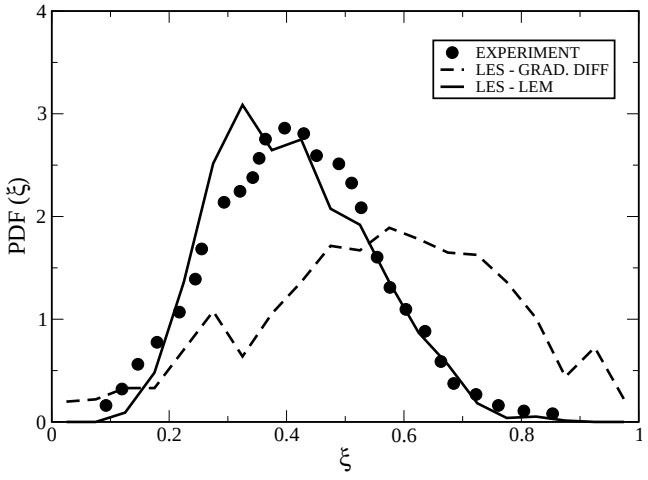

b) $M_C = 0.62$

Figure 7 PDF of the mixture fraction.